Physically activated wheat straw-derived biochar for biomass pyrolysis vapors upgrading with high resistance against coke deactivation

Christian Di Stasi*, Darío Alvira, Gianluca Greco, Belén González, Joan J. Manyà

Aragón Institute of Engineering Research (I3A), Technological College of Huesca, University of Zaragoza, crta. Cuarte s/n, Huesca E-22071, Spain

* Corresponding author at: *Aragón Institute of Engineering Research (I3A), Technological College of Huesca, University of Zaragoza, crta. Cuarte s/n, Huesca E-22071, Spain.*

E-mail address: christiandistasi@unizar.es.

ABSTRACT

Wheat straw-derived biochars (produced through slow pyrolysis at 500 °C and 0.1 MPa) were physically (with CO_2) and chemically (with K_2CO_3) activated to assess their performance as renewable and low-cost catalysts for biomass pyrolysis vapors upgrading. Preliminary cracking experiments, which were carried out at 700 °C using a mixture of four representative model compounds, revealed a clear correlation between the volume of micropores of the catalyst and the total gas production, suggesting that physical activation up to a degree of burn-off of 40% was the most interesting activation route. Next, steam reforming experiments were conducted using the most microporous material to analyze the effect of both the bed temperature and gas hourly space velocity (GHSV) on the total gas production. The results showed a strong dependence between the bed temperature and the total gas production, with the best result obtained at the highest temperature (750 °C). On the other hand, the change in GHSV led to minor changes in the total gas yield, with a maximum achieved at 14500 h^{-1}. Under the best operating conditions deduced in the previous stages, the addition of CO_2 into the feed gas stream (partial pressure of 20 kPa) resulted in a total gas production of 98% with a H_2/CO molar ratio of 2.16. This good result, which was also observed during the upgrading of the aqueous phase of a real biomass pyrolysis oil, was ascribed to the relatively high coke gasification rate, which refresh the active surface area preventing deactivation by coke deposition.

KEYWORDS

Activated biochar; wheat straw; pyrolysis vapor upgrading; model compounds; molar H_2/CO ratio.

1. Introduction

It is widely recognized that slow pyrolysis is the thermochemical process by which the yield of biochar is maximized (around 25–35 wt. %, depending on the feedstock and operating conditions) [1]. The effluent stream from the pyrolysis process is composed of a fraction of permanent gases (CO_2, CO, CH_4, H_2, and light hydrocarbons), water and condensable organic compounds. After condensation, the resulting product, which is often referred to as "bio-oil"[2] or "pyrolysis oil" [3,4], consists of a mixture of water and oxygen-containing organic compounds (e.g., carboxylic acids, phenols, alcohols, aldehydes, ketones and furans [5–7]) derived from the thermal decomposition of major biomass components. Despite the fact that pyrolysis oil can be upgraded to liquid fuel by means of complex deoxygenation and hydrogenation processes [8], a practical approach to avoid undesirable condensation of volatiles (which causes operational issues in the downstream applications of the pyrolysis gas) is their conversion to permanent gases via cracking and steam/dry reforming, either thermally or catalytically.

Using a feasible catalyst in the pyrolysis vapor upgrading process is essential to reach high conversion levels with an appropriate selectivity to the desired products. So far, metal-based catalysts (mainly Ni [9,10], and, to a lesser extent, some transition metals such as Fe [11] and Co [12]) have been investigated for this purpose. In the last years, a growing interest in using biochar as catalyst or catalyst support has arisen [10,13–15]. The reason is that biochar is a versatile material that can further be upgraded by activation and/or functionalization processes [16–20]. Furthermore, using biochar as catalysts for pyrolysis vapors upgrading could offer practical advantages, such as higher resistance to deactivation by carbon deposition (due to the extent of both steam and CO_2 gasification reactions [12,21]) and the fact that spent biochar-based catalysts can be directly gasified or burnt to recover energy [22].

The performance of a catalyst generally depends on its textural properties. Indeed, an appropriate value of surface area guarantees a high level of interaction between the reactants and the active sites. In any case, pristine biochar has a relatively low specific surface area, which is generally dominated by narrow micropore contributions [23,24]. Therefore, an activation step is required to expand the initial porosity of biochar and thus, facilitating high mass transfer fluxes and high active loadings.

Activation processes are generally classified as either physical or chemical, depending on the activation procedure. Physical activation is the process in which the development of porosity is obtained through controlled gasification of carbon, using an oxidizing agent such as CO_2, H_2O or O_2 [25,26]. When the activation of biochar is obtained by means of a chemical agent that improves the gasification rate, the process is considered a chemical activation. The most used chemicals in literature are H_3PO_4, $ZnCl_2$, KOH, and NaOH, but all of them have drawbacks. For instance, H_3PO_4 [27] and $ZnCl_2$ [28] are hardly retrieved from the spent biochar, leading to eutrophication and heavy metal pollution [29]. On the other hand, KOH [30] and NaOH [31] are strong corrosive substances and their use in large-scale processes is not feasible. An interesting alternative is the use of K_2CO_3 since it has proven to be an effective chemical agent [32–34] and represents a more suitable material for scale-up purposes.

The specific aim of this study is to assess the suitability and performance (in terms of total gas yield, H_2/CO molar ratio, and resistance to deactivation) of wheat straw-derived activated biochars to be used as renewable and low-cost catalysts for pyrolysis vapors upgrading processes. Two biochar activation procedures (physical activation with CO_2 and chemical activation with K_2CO_3) were performed to identify which one was the most appropriate for the purpose of this work. Due to the complex composition of the real pyrolysis oil, a mixture of four biomass pyrolysis vapor model compounds (acetic acid, acetone, ethanol and eugenol) was used during the most part of the study in order to ensure reproducible results. The first two

compounds are typically released during the pyrolysis of hemicelluloses and cellulose, whereas the last two are linked to the decomposition of lignin [7,35]. Similar model compounds were already employed in earlier studies [36–38]. Finally, for validation purposes, the last experimental stage was undertaken using the real bio-oil aqueous-phase produced during the slow pyrolysis of wheat straw pellets.

2. Experimental section

2.1. Production of biochar

The biochar employed in this work was obtained from binder-free wheat straw pellets (9 mm OD and 10–13 mm long), which were provided by a Belgian company. Biochar was produced via slow pyrolysis (at an average heating rate of 5 °C min^{-1}) using a bench-scale fixed-bed reactor (the description of which is available in previous studies [24,39]), at a highest temperature of 500 °C, a soaking time (at 500 °C) for the solid fraction of 60 min and a residence time of the carrier gas (N_2) within the reactor of 100 s. We chose these operating conditions in light of a previous study [24], where they were suggested as appropriate conditions to reach a reasonable compromise between the yield of biochar and its properties in terms of potential stability. The produced biochar (referred as "RW") was crushed and sieved to obtain particle sizes within the range of 0.212–1.41 mm.

Both the wheat straw pellets and the raw biochar were characterized by proximate and ultimate (CHN) analyses. Proximate analyses were conducted in quadruplicate according to ASTM standards. An elemental analyzer, model CHN628 from Leco Corporation (USA), was used for ultimate analyses, which were performed in triplicate. Furthermore, X-Ray Fluorescence (XRF) spectroscopy analysis (ADVANT'XP+XRF spectrometer from Thermo ARL, Switzerland) were carried out to evaluate the inorganic content of the ashes present in the biomass and raw biochar.

2.2. Activation of biochar

Physical and chemical activations were conducted using a tubular quartz reactor (600 mm long and 17.5 mm ID), which was placed inside a vertical tubular furnace (model EVA 12/300 from Carbolite Gero, UK). The temperature inside the bed was monitored by means of a K-type thermocouple placed along the longitudinal axis of the reactor. A schematic diagram of the activation set-up is given in Fig. A.1 (Appendix 1: Supplementary Data).

The production of physically activated biochars was carried out under a pure CO_2 atmosphere at 800 °C. A sample of 10 g of raw biochar (RW) was heated under N_2 atmosphere (500 mL min^{-1} STP) at a heating rate of 10 °C min^{-1}. Once the target temperature (800 °C) was reached, the gas feed was switched from N_2 to CO_2. Under these conditions, the gas-hourly space velocity (GHSV) was estimated to be 6500 h^{-1}. The activation soaking time (under CO_2 atmosphere at 800 °C) was modified to obtain different degrees of burn-off (BO), which is defined in Eq. (1). In such equation, m_0 and m_f correspond to the initial mass of biochar and the final mass of activated biochar, respectively, whereas α is the devolatilization ratio (i.e., mass loss fraction of RW biochar after heating up to 800 °C under pure N_2), which in this work resulted to be equal to 0.12.

$$\mathrm{BO} = \left[\frac{m_0(1-\alpha) - m_f}{m_0(1-\alpha)}\right] 100 \quad (1)$$

Regarding the chemical activation, the RW biochar was impregnated with an aqueous solution of K_2CO_3 (2 M) at a mass ratio K_2CO_3/biochar of 1/1. The heterogeneous mixture was stirred for 2 h at 60 °C to improve the diffusion of the agent into the solid. Then, the liquid phase was removed by filtration, and the biochar dried at 110 °C overnight. Afterward, the resulted impregnated biochar was heated up to 700 °C at a heating rate of 10 °C min^{-1} under inert atmosphere (N_2). The sample was kept at the final temperature for 1 h and cooled down to room temperature. The relatively low temperature (700 °C) used in chemical activation was chosen to avoid losses of metallic potassium due to its vaporization, which occurs at 760 °C

[40]. Finally, the solid product was washed with hot deionized water followed by dilute HCl (0.5 M) to remove the excess of inorganic salts and dried at 110 °C overnight.

Besides its role as precursor, the catalytic activity of the non-activated biochar was also assessed in the catalytic cracking of a mixture of model compounds. In order to prevent any structural modification during the catalytic process, the RW biochar was heated at 10 °C min^{-1} under N_2 atmosphere up to 800 °C for 1 h (using the same device previously described). The resulting devolatilized biochar is referred as "BC".

Table 1 summarizes the nomenclature used to designate the activated and non-activated biochars.

2.3. Textural characterization

N_2 adsorption isotherms at –196 °C were performed to determine the specific surface area and pore size distribution (PSD) of both non-activated and activated biochars. A gas sorption analyzer, model ASAP2020 from Micromeritics (USA), was used for this purpose. Samples (120 mg) were previously degassed under dynamic vacuum conditions at 150 °C to remove water and other impurities. The specific surface area (S_{BET}) was obtained using the BET model, whereas the total pore volume (V_t) was determined from the amount of N_2 adsorbed at high relative pressure (p/p_0 = 0.98–0.99). The micropore volume (V_{mic}) was evaluated using the *t*-plot method. The PSD (excluding narrow micropores) was estimated assuming a Non-Local Density Functional Theory (NLDFT) model and slit-pore geometry. Then, the volume of mesopores (V_{meso}) was determined by subtracting the V_{mic} from the cumulative pore volume up to 50 nm. To determine the volume of narrow micropores (i.e., ultra-micropores) and the corresponding PSD for the range 0.3–1.0 nm [41,42], CO_2 adsorption isotherms at 0 °C were also performed. The volume of ultra-micropores (V_{ultra}) was then determined using conventional Density Functional Theory (DFT) and assuming slit-pore geometry.

2.4. Cracking and reforming experiments

The performance of the activated and non-activated biochars during cracking/reforming of pyrolysis vapors was tested in a bench-scale device. The core of the system was a fixed-bed reactor (10 mm ID and 300 mm long) made in Hastelloy C276 (EN 2.4819), in which 5 g of solid was loaded. The reactor was heated by a PID controlled electric furnace. A K-type thermocouple was placed within the packed bed. The pressure drop between the inlet and the outlet of the reactor was monitored with a differential pressure transmitter. The liquid reactant feed was introduced using an HPLC pump (model 521 from Analytical Scientific Instruments, USA) and then evaporated in a heater. For cracking experiments, an equal-mass mixture of the four model compounds (acetic acid, acetone, ethanol, and eugenol) was used as feed liquid and, for reforming tests, deionized water was added to the above-mentioned mixture, resulting in a feed liquid composed of 50 wt. % of water. The resulting vapor stream was then mixed with the gas feed (N_2 or N_2/CO_2). The reactor outlet stream, which was composed of permanent gases and condensable compounds, was cooled down in a condensation train (composed of 3 Drechsel bottles placed in an ice bath). Permanent gases were analyzed using a dual channel micro-gas chromatograph (μ-GC 490 from Agilent, USA) equipped with TCD detectors and two analytical columns (a Molsieve 5 A and a PolarPlot U). The known amount of N_2 fed was used as tracking compound to calculate the mass of produced gas. Fig. 1 shows a schematic overview of the experimental device.

The total gas production (Y_g), as defined by Eq. (2), was chosen as a measure of the performance of the upgrading experiments. The selection of this parameter instead of the more common liquid conversion was due to the difficulties in recovering the total amount of condensable products from the reactor effluent. Since highly volatile compounds were present in the condensable fraction, a considerable amount of them could leave the system in the vapor phase. This was confirmed by the results obtained from a simulation study using Aspen Plus

(more details are available in Fig. A.2 and Table A.1). Besides the total gas production, the yields of individual gas species (η_i) were determined according to Eq. (3).

$$Y_g = \frac{m_g}{m_L} 100 \quad (2)$$

$$\eta_i = \frac{n_i}{m_L} \quad (3)$$

In Eqs. (2) and (3), m_g is the mass of produced gas (in grams), m_L the mass of liquid fed into the reactor (in g, dry basis) and n_i the amount produced of a given gas species (in mmol). It should be pointed out that values of Y_g greater than 100% can be obtained for reforming experiments, since the variable m_L does not include the mass of water fed.

To assess the catalytic activity of the wall of the reactor and/or the extent of thermal cracking of the liquid fed, two types of blank tests were firstly carried out: one using an empty reactor and the other one using a bed of silica sand. Catalytic cracking experiments were then conducted to choose the best activated biochar (in terms of Y_g) keeping constant the operating conditions (i.e., bed temperature and GHSV). In a second stage, steam reforming (SR) tests were performed using the best catalyst under different bed temperatures and GHSV values. Next, steam and dry reforming (SDR) tests were carried out (for the best catalyst and the best operating conditions deduced from SR tests) using a mixture of N_2 and CO_2 (at different CO_2 partial pressures) as feed gas stream. Since CO_2 was both a reactant and product in the reactions involved in the process, the Y_g and η_{CO2} values were calculated considering the net mass of CO_2 (i.e., the amount at the outlet minus the amount fed). The final stage of the experimental study consisted on the steam and dry reforming of the aqueous fraction of a real pyrolysis oil. To this end, we used the bio-oil aqueous-phase produced during the slow pyrolysis of wheat straw pellets at 500 °C and 0.1 MPa. The water content of the liquid fed was measured by Karl Fischer titration. A summary of the experimental tests and their operating conditions is given in Table 2.

3. Results and discussion

To guarantee a reasonable degree of reliability of the experimental results obtained from the used set-up, the repeatability of measurements was assessed by comparing three replicates of a given steam and dry reforming experiment (not reported in Table 2). The results from these repeated tests, which are summarized in Table A.2, showed an acceptable degree of repeatability.

3.1. Properties of the produced biochars

The results of the proximate, ultimate and XRF analyses of wheat straw biomass and pristine biochar (RW) are reported in Table A.3. For physically activated biochars at 800 °C, the desired degrees of burn-off (15%, 30%, and 40%) were reached by adjusting the soaking times at 30, 45 and 60 min, respectively.

The main results from the textural characterization of activated and non-activated biochars are reported in Table 3. For the non-activated biochar (BC), the extremely low (near zero) S_{BET} value and non-detectable pore volumes deduced from the N_2 adsorption isotherm at –196 °C can be explained by the fact that porosity is dominated by narrow micropores (i.e., ultra-micropores; pore sizes below 0.7 nm). At cryogenic temperatures, the diffusion rate of N_2 into ultra-micropores becomes extremely slow [42].

For the chemically activated biochar (CAC), the specific surface area (89.0 $m^2\ g^{-1}$, from N_2 isotherm) was significantly lower than the values found in the literature [29]. Since most of the previous studies impregnated biomass instead of biochar, a possible explanation of this low surface area could be due the hydrophobicity of the precursor used here (low atomic O:C ratio, as reported in Table A3 [43]), which hindered the diffusion of the aqueous solution into the solid bulk. Furthermore, the relatively low final activation temperature (700 °C) could not be high enough to obtain an appropriate extent of reaction.

On the other hand, physically activated biochars exhibited appropriate specific surface areas and pore volumes (see Table 3). In addition, an increase in the degree of burn-off from 15% to

30% and 40% led to a progressive and marked increase in the specific surface area, which was mainly attributed to the development of new micropores. This is in good agreement with earlier studies available in the literature [44,45].

3.2. Catalytic cracking experiments

The cracking process mainly involves the decomposition of volatile organic compounds through successive reactions (the main of which are listed in Table 4), leading to the production of lighter compounds and permanent gases. In addition, coke can be formed through polymerization reactions of free radicals released during cracking. The deposition of coke on the catalyst surface can result in a fast deactivation of the catalyst by pore plugging [46,47].

The performance of all the catalysts tested during the cracking experiments (which were conducted at 700 °C and at a GHSV of 19500 h^{-1}) is shown in Fig. 2. For the two blank experiments (not displayed in Fig. 2), the total gas production (Y_g) was very low (6.1% and 7.4% using an empty reactor and a bed of silica sand, respectively), suggesting that both the catalytic effect of the reactor wall and the model mixture degradation (due to thermal cracking) were negligible under the operating conditions used here.

As can be seen in Fig. 2a, the total gas production obtained using the non-activated biochar (BC) was around 22%. Despite the fact that the value of Y_g was relatively low, it was considerably higher than that obtained using a bed of silica sand. This can indicate that, given the extremely low porosity of the non-activated biochar, the presence of inherent inorganic species available on their surface, especially K and Ca (see Table A.3), could lead to a certain catalytic activity [48,49]. On the other hand, slightly better results were obtained for physically activated biochar at mild conditions (BO = 15%).

As expected, in accordance with the textural properties reported in Table 3, an increase in the degree of burn-off led to a progressive increase in the total gas production, which reached a maximum of 40% for the PAC40 catalyst (which had the highest V_{mic}). As it is also shown in

Fig. 2a, the yields of produced CH_4, CO_2 and CO significantly increased with the degree of burn-off; however, the yield of H_2 was relatively low and almost constant for all experiments.

With regard to the chemically activated biochar (CAC), its catalytic activity was much lower than that observed for physically activated biochars. A total gas production of only 14% was obtained when a bed of this material was used. This poor performance (which was even lower than that measured for non-activated biochar) could be explained by the lack of microporous and the fact that the washing step with dilute HCl (performed at the end of the chemical activation process) led to a certain removal of the inorganic species from the biochar [50] and, consequently, an inhibition of the above-mentioned inherent catalytic activity. Indeed, such hypothesis was confirmed by XRF analysis of CAC ashes, which revealed that potassium content drastically decreased from 12.29 wt. % of the RW ashes to 3.69 wt. % of the acid-washed chemically activated biochar (CAC).

Fig. 2b compares the time evolution of the H_2 production rates for the cracking experiments conducted using activated biochars. From this figure, it can be deduced a relatively fast deactivation (occurring during the first 10 min of operation) of BC, CAC and, PAC15 catalysts. However, a slightly higher resistance to deactivation by coke deposition was observed for physically activated biochars at high degrees of burn-off (30% and 40% for PAC30 and PAC40, respectively), probably due to their higher initial microporosity [51].

In summary, one can conclude that physical activation up to a relatively high degree of burn-off (i.e., PAC40) was the most appropriate way to produce a biochar-derived catalyst, since cracking reactions were enhanced due to the relatively higher specific surface area and micropores content. Thus, the PAC40 catalyst was selected for the next experimental steps.

3.3. Catalytic steam reforming

In this experimental stage, a preliminary blank test was performed to measure the effect of the presence of water in the feed stream on the thermal stability of the mixture of model

compounds. This test, which was conducted using a bed of silica sand at 700 °C and a GHSV of 19500 h^{-1}, resulted in a total gas production of only 6.0%. Therefore, the extent of uncatalyzed cracking and/or reforming reactions was negligible, even in the presence of water.

As expected, the addition of water led to an increase in the total gas production and sharp differences in the yields of gaseous species. As shown in Fig. 3a, the steam reforming (SR) test conducted using the PAC40 catalyst under the same conditions than those used for the catalytic cracking test (700 °C and a GHSV of 19500 h^{-1}) revealed a marked increase in the production of H_2 (and, to a lesser extent, CO_2) at the expense of CO and CH_4. A possible explanation for this finding is the fact that the water fed into the reactor was not only involved in reforming reactions (reactions 2 and 3 in Table 4), but also helped to keep the catalyst active through steam gasification of both the catalyst and formed coke (reaction 6 in Table 4) [12,48]. In addition, and as pointed out by Feng et al. [49], the oxidative nature of steam can lead to the formation of O-containing functional groups and related crystal lattice defects, which could provide further active sites for gasification. Because of the simultaneous deposition and gasification of coke, larger fluctuations in the pressure drop across the bed (in comparison with cracking experiments) were observed, as shown in Fig. A.3. On the other hand, the relatively low production of CO could be related to a promotion of the water-gas-shift reaction (reaction 4 in Table 4), which also leads to an additional production of CO_2 [50].

Concerning the effect of the gas-hourly space velocity, four SR tests at different values of GHSV were performed. From the results shown in Fig. 3a, it can be seen that the highest yield of H_2 (as well as Y_g) was obtained at 14500 h^{-1}. Earlier studies (see, for instance, the study by Hu et al. [52]) have reported a progressive increase in the total gas production as the gas residence time increased. However, a slight decrease in the total gas production (and yield of H_2) was observed at the lowest GHSV tested (12000 h^{-1}). This apparently contradictory result might be related to a higher extent of polymerization reactions at longer contact times, leading

to excessive coke deposition. This is consistent with the slightly faster deactivation shown in Fig. 3b for the SR test conducted at the lowest GHSV. In view of these results, a GHSV of 14500 h^{-1} was chosen as the most appropriate for subsequent experiments.

With regard to the influence of the bed temperature, four additional SR tests were performed at 600, 650, 700 and 750 °C, keeping constant the GHSV at the best value deduced above. As can be observed in Fig. 4a, the total gas production was strongly dependent on the reforming temperature. As the temperature increased, it was observed a marked enhancement in the production of H_2 and, to a much lesser extent, CO_2, CO, and CH_4. Both the highest total gas production and yield of H_2 were maximized at the highest temperature tested (750 °C). Fig. 4b also shows that, at this temperature, the PAC40 exhibited a good resistance to deactivation. This finding seems to confirm that, at 750 °C, the rate of the steam gasification reaction was high enough to compensate for the deposition of coke on the surface of the catalyst. To gain additional insights on the porosity evolution, the catalysts used in SR tests conducted at 700 and 750 °C were analyzed in terms of S_{BET} and PSD. As expected, the spent catalysts exhibited differences in the specific surface area and PSD in comparison with the fresh ones, as illustrated in Fig. 5. The lower decrease in the S_{BET} observed for the spent catalyst at 750°C (a 31% decrease instead of a 58% for the catalyst used at 700 °C) could be related to the higher extent of the steam gasification reaction and subsequent further development of new pores. In addition, the spent biochars exhibited lower volumes of micropores (following the same trend observed for the S_{BET}); however, the volume of mesopores increased of 17% when the catalyst was tested at 750 °C.

3.4. Catalytic steam and dry reforming

Since the pyrolysis outlet stream always contains CO_2, more realistic steam and dry reforming (SDR) experiments are required. In addition, considerably lower H_2/CO ratios, in comparison with those obtained using steam reforming (which are too high for most

applications [54]), can be obtained by feeding a certain amount of CO_2. The results obtained from SDR experiments performed at different partial pressures of CO_2 in the feed gas stream, under the best operating conditions deduced in the previous section and using the PAC40 catalyst are presented and discussed here.

As shown in Fig. 6a, the addition of CO_2 into the feed gas stream induced a progressive increase in the total gas production (Y_g). This was largely due to the promotion of dry reforming reactions as well as the reverse Boudouard reaction (reactions 5 and 7 in Table 4). Nevertheless, a certain decrease in the yield of H_2 was also observed when the highest amount of CO_2 (p_{CO2} = 30 kPa) was fed into the reactor. This finding could be explained by the fact that a higher CO_2 partial pressure can result in a higher extent of dry reforming at the expense of steam reforming, leading to a lower production of H_2. Similarly, the reverse Boudouard reaction could also be enhanced further, resulting in a lower steam gasification rate. In view of the results obtained from the SDR tests, we can conclude that a CO_2 partial pressure of 20 kPa in the feed gas stream can be considered as the best condition tested, since it provided the highest yield of H_2 (26.5 mmol g^{-1} with a composition in the produced gas of 46.5 vol. %) and a molar H_2/CO ratio in the produced gas of 2.15, which was close to the optimal value for Fischer-Tropsch synthesis (2.00) [53,54].

A comparison of the resistance to deactivation of the PAC40 catalyst, working under the best reaction conditions for both SR and SDR processes, is given in Fig. 6b. As can be deduced from the time evolution of the instantaneous production of H_2, the addition of CO_2 into the gas feed resulted in an apparently improved resistance to coke formation. This finding was expected, since CO_2 can increase further the availability of defects in the biochar, which results in an enhanced reactivity towards steam and CO_2 gasification [49].

3.5. Real pyrolysis oil

The aqueous fraction of the bio-oil produced during the pyrolysis of wheat straw at the highest temperature of 500 °C and at 0.1 MPa was filtered and fed into the reformer. The best process operating conditions deduced from the SDR tests (for the mixture of model compounds) were selected for the catalytic upgrading of the real bio-oil sample. As can be seen in Fig. 7a, both the total gas production and yield of H_2 were improved when the real bio-oil sample was used instead of the mixture of model compounds. This finding could partly be explained by differences in composition between the two liquid feedstocks. In this sense, the real bio-oil sample could contain a higher fraction of light volatile compounds, which are more susceptible to thermal decomposition. Furthermore, the content of water in the bio-oil sample was considerably higher than that of the wet mixture of model compounds (75.6 vs. 50 wt. %). The resulting increased amount of water could lead to a greater extent of the water-consuming reactions (e.g., WGS and steam reforming reactions), therefore resulting in increased yields of H_2 and CO_2 at the expense of CO and CH_4, as displayed in Fig. 7a.

Regarding the stability of the PAC40 catalysts during the upgrading of the real bio-oil sample, Fig. 7b reveals a good resistance to deactivation over the course of a 60-min experiment. In fact, the behavior observed was very similar to that seen previously for the upgrading of the mixture of model compounds.

In summary, the results reported here indicate that physically activated wheat-straw derived biochars are appropriate for the upgrading of biomass pyrolysis vapors. It should be highlighted that the best performing activated biochar (PAC40) exhibited a good catalytic activity and resistance to deactivation by coke deposition at 750 °C (a moderate temperature for a non-metal-based catalyst) and with a low residence time within the catalyst bed (0.25 s). Further studies are needed to assess the long-term stability of biochars as well as the ability of such activated biochars to upgrade real pyrolysis vapors in a downstream fixed-bed reactor.

4. Conclusions

From the analysis of the results mentioned above, the following conclusions can be drawn:

(1) Wheat straw-derived biochars activated with CO_2 at 800 °C, up to a degree of burn-off of 40%, showed an appropriate specific surface area, which was mostly attributed to micropores.

(2) The good catalytic activity and stability observed for the best activated biochar (i.e., 40% BO) during the upgrading of a mixture of model compounds could be explained by three reasons: (*i*) the availability of alkali metals (e.g., K) on the surface of the char matrix, (*ii*) the high surface area and microporous volume obtained through biochar physical activation, and (*iii*) the oxidizing nature of steam and CO_2, which can result in the formation of crystal lattice defects. In all cases, the number of active sites on the surface of biochar can increase, leading to an enhancement of the biochar gasification reactivity. The higher extent of both steam gasification and reverse Boudouard reactions can help to refresh the active surface area and therefore prevent deactivation by coke deposition.

(3) The good results also obtained for an aqueous fraction of a real biomass pyrolysis oil seem to confirm the ability of the best activated biochar for upgrading purposes. Despite the fact that the process temperature used here was not so high (750 °C), further research should focus on lowering it. To this end, developing K-loaded activated biochars appears to be an interesting option.

Acknowledgments

This project received funding from the European Union's Horizon 2020 research and innovation programme under the Marie Skłodowska-Curie grant agreement No 721991. The authors also acknowledge the funding from the Aragón Government (Ref. T22_17R), co-funded by FEDER 2014-2020 "Construyendo Europa desde Aragón".

Appendix A. Supplementary data

Figs. A.1, A.2, A.3. Tables A.1, A.2, and A.3.

Nomenclature

BO	Degree of burn-off for the physically activated biochars (%)
m_0	Initial mass of biochar before activation (g)
m_g	Mass of produced gas during the upgrading process (g)
m_f	Final mass of biochar after activation (g)
m_L	Mass of liquid fed into the upgrading reactor (g)
n_i	Produced amount of a given gas specie (mmol)
S_{BET}	Brunauer-Emmett-Teller specific surface area ($m^2\ g^{-1}$)
V_{meso}	Volume of mesopores ($cm^3\ g^{-1}$)
V_{mic}	Volume of micropores ($cm^3\ g^{-1}$)
V_t	Total pores volume ($cm^3\ g^{-1}$)
V_{ultra}	Volume of ultra-micropores ($cm^3\ g^{-1}$)
Y_g	Total gas production (%)

Greek symbols

α	Fraction of mass loss of raw biochar after heating up to 800 °C under N_2 (–)
η_i	Yield of individual produced gas components ($mmol\ g^{-1}$)

Acronyms

GHSV	Gas hourly space velocity
NLDFT	Non-local density functional theory
SDR	Steam and dry reforming
SR	Steam reforming

PSD	Pore size distribution
TCD	Thermal conductivity detector
μ-GC	Micro gas chromatograph
WGS	Water gas shift

References

[1] Manyà JJ. Pyrolysis for Biochar Purposes: A Review to Establish Current Knowledge Gaps and Research Needs. Environ Sci Technol 2012;46:7939–54. https://doi.org/10.1021/es301029g.

[2] Mourant D, Hasan MDM, Song Y, Li C-Z, Hu X, Gunawan R, et al. Upgrading of bio-oil via acid-catalyzed reactions in alcohols — A mini review. Fuel Process Technol 2016;155:2–19. https://doi.org/10.1016/j.fuproc.2016.08.020.

[3] Mahyoub SAA, Liao W, Ma P, Zhao H, Guo M, Li H, et al. Effect of pyrolysis temperature on characteristics and aromatic contaminants adsorption behavior of magnetic biochar derived from pyrolysis oil distillation residue. Bioresour Technol 2016;223:20–6. https://doi.org/10.1016/j.biortech.2016.10.033.

[4] Oasmaa A, Fonts I, Pelaez-Samaniego MR, Garcia-Perez ME, Garcia-Perez M. Pyrolysis Oil Multiphase Behavior and Phase Stability: A Review. Energy Fuels 2016;30:6179–200. https://doi.org/10.1021/acs.energyfuels.6b01287.

[5] Oasmaa A, Kuoppala E, Solantausta Y. Fast pyrolysis of forestry residue. 2. Physicochemical composition of product liquid. Energy Fuels 2003;17:433–43. https://doi.org/10.1021/ef020206g.

[6] Fraga AR, Gaines AF, Kandiyoti R. Characterization of biomass pyrolysis tars produced in the relative absence of extraparticle secondary reactions. Fuel 1991;70:803–9. https://doi.org/10.1016/0016-2361(91)90186-E.

[7] Yang Z, Kumar A, Huhnke RL, Buser M, Capareda S. Pyrolysis of eastern redcedar: Distribution and characteristics of fast and slow pyrolysis products. Fuel 2016;166:157–65. https://doi.org/10.1016/j.fuel.2015.10.101.

[8] Lu Q, Li WZ, Zhu XF. Overview of fuel properties of biomass fast pyrolysis oils. Energy Convers Manag 2009;50:1376–83. https://doi.org/10.1016/j.enconman.2009.01.001.

[9] Hornung U, Schneider D, Hornung A, Tumiatti V, Seifert H. Sequential pyrolysis and catalytic low temperature reforming of wheat straw. J Anal Appl Pyrolysis 2009;85:145–50. https://doi.org/10.1016/j.jaap.2008.11.006.

[10] Shen Y, Zhao P, Shao Q, Ma D, Takahashi F, Yoshikawa K. In-situ catalytic conversion of tar using rice husk char-supported nickel-iron catalysts for biomass pyrolysis/gasification. Appl Catal B Environ 2014;152–153:140–51. https://doi.org/10.1016/j.apcatb.2014.01.032.

[11] Xiang J, Liu Q, Deng Z, Wang Y, Su S, Hu S, et al. Effect of the pre-reforming by Fe/bio-char catalyst on a two-stage catalytic steam reforming of bio-oil. Fuel 2018;239:282–9. https://doi.org/10.1016/j.fuel.2018.11.029.

[12] Hosokai S, Norinaga K, Kimura T, Nakano M, Li C-Z, Hayashi J. Reforming of Volatiles from the Biomass Pyrolysis over Charcoal in a Sequence of Coke Deposition and Steam Gasification of Coke. Energy Fuels 2011;25:5387–93. https://doi.org/10.1021/ef2003766.

[13] Shen Y, Chen M, Sun T, Jia J. Catalytic reforming of pyrolysis tar over metallic nickel nanoparticles embedded in pyrochar. Fuel 2015;159:570–9. https://doi.org/10.1016/j.fuel.2015.07.007.

[14] Wang Y, Jiang L, Hu S, Su S, Zhou Y, Xiang J, et al. Evolution of structure and activity of char-supported iron catalysts prepared for steam reforming of bio-oil. Fuel Process Technol 2017;158:180–90. https://doi.org/10.1016/j.fuproc.2017.01.002.

[15] Mani S, Kastner JR, Juneja A. Catalytic decomposition of toluene using a biomass derived catalyst. Fuel Process Technol 2013;114:118–25. https://doi.org/10.1016/j.fuproc.2013.03.015.

[16] Xue Y, Gao B, Yao Y, Inyang M, Zhang M, Zimmerman AR, et al. Hydrogen peroxide modification enhances the ability of biochar (hydrochar) produced from hydrothermal carbonization of peanut hull to remove aqueous heavy metals: Batch and column tests. Chem Eng J 2012;200–202:673–80. https://doi.org/10.1016/J.CEJ.2012.06.116.

[17] Jimenez-Cordero D, Heras F, Alonso-Morales N, Gilarranz MA, Rodriguez JJ. Ozone as oxidation agent in cyclic activation of biochar. Fuel Process Technol 2015;139:42–8. https://doi.org/10.1016/j.fuproc.2015.08.016.

[18] Feng W, Kwon S, Borguet E, Vidic R. Adsorption of hydrogen sulfide onto activated carbon fibers: Effect of pore structure and surface chemistry. Environ Sci Technol 2005;39:9744–9. https://doi.org/10.1021/es0507158.

[19] Titirici MM, Thomas A, Antonietti M. Aminated hydrophilic ordered mesoporous carbons. J Mater Chem 2007;17:3412–8. https://doi.org/10.1039/b703569a.

[20] Pérez-Cadenas AF, Maldonado-Hódar FJ, Moreno-Castilla C. On the nature of surface acid sites of chlorinated activated carbons. Carbon 2003;41:473–8. https://doi.org/10.1016/S0008-6223(02)00353-6.

[21] Abu El-Rub Z, Bramer EA, Brem G. Experimental comparison of biomass chars with other catalysts for tar reduction. Fuel 2008;87:2243–52. https://doi.org/10.1016/j.fuel.2008.01.004.

[22] Shen Y. Chars as carbonaceous adsorbents/catalysts for tar elimination during biomass pyrolysis or gasification. Renew Sustain Energy Rev 2015;43:281–95. https://doi.org/10.1016/j.rser.2014.11.061.

[23] Manyà JJ, González B, Azuara M, Arner G. Ultra-microporous adsorbents prepared from vine shoots-derived biochar with high CO2 uptake and CO2/N2 selectivity. Chem Eng J 2018;345:631–9. https://doi.org/10.1016/j.cej.2018.01.092.

[24] Greco G, Videgain M, Di Stasi C, González B, Manyà JJ. Evolution of the mass-loss rate during atmospheric and pressurized slow pyrolysis of wheat straw in a bench-scale reactor. J Anal Appl Pyrolysis 2018;136:18–26. https://doi.org/10.1016/j.jaap.2018.11.007.

[25] Molina-Sabio M, González MT, Rodriguez-Reinoso F, Sepúlveda-Escribano A. Effect of steam and carbon dioxide activation in the micropore size distribution of activated carbon. Carbon 1996;34:505–9. https://doi.org/10.1016/0008-6223(96)00006-1.

[26] Plaza MG, González AS, Pis JJ, Rubiera F, Pevida C. Production of microporous biochars by single-step oxidation: Effect of activation conditions on CO2 capture. Appl Energy 2014;114:551–62. https://doi.org/10.1016/j.apenergy.2013.09.058.

[27] Lillo-Rodenas MA, Fletcher AJ, Thomas KM, Cazorla-Amoros D, Linares-Solano A. Competitive adsorption of a benzene-toluene mixture on activated carbons at low concentration. Carbon 2006;44:1455–63. https://doi.org/10.1016/j.carbon.2005.12.001.

[28] Sun K, Huang Q, Chi Y, Yan J. Effect of ZnCl2-activated biochar on catalytic pyrolysis of mixed waste plastics for producing aromatic-enriched oil. Waste Manage 2018; 81:128-137. https://doi.org/10.1016/j.wasman.2018.09.054.

[29] Tsai WT, Chang CY, Wang SY, Chang CF, Chien SF, Sun HF. Preparation of activated carbons from corn cob catalyzed by potassium salts and subsequent gasification with CO2. Bioresour Technol 2001;78:203–8. https://doi.org/10.1016/S0960-8524(00)00111-5.

[30] Dehkhoda AM, Gyenge E, Ellis N. A novel method to tailor the porous structure of KOH-activated biochar and its application in capacitive deionization and energy storage. Biomass Bioenergy 2016;87:107–21. https://doi.org/10.1016/j.biombioe.2016.02.023.

[31] Tseng RL. Physical and chemical properties and adsorption type of activated carbon prepared from plum kernels by NaOH activation. J Hazard Mater 2007; 147(3):1020-7 https://doi.org/10.1016/j.jhazmat.2007.01.140.

[32] Adinata D, Wan Daud WMA, Aroua MK. Preparation and characterization of activated carbon from palm shell by chemical activation with K2CO3. Bioresour Technol 2007;98:145–9. https://doi.org/10.1016/j.biortech.2005.11.006

[33] Foo KY, Hameed BH. Utilization of rice husks as a feedstock for preparation of activated carbon by microwave induced KOH and K2CO3activation. Bioresour Technol 2011;102:9814–7. https://doi.org/10.1016/j.biortech.2011.07.102.

[34] Hayashi J, Horikawa T, Takeda I, Muroyama K, Nasir Ani F. Preparing activated carbon from various nutshells by chemical activation with K2CO3. Carbon 2002;40:2381–6. https://doi.org/10.1016/S0008-6223(02)00118-5

[35] Mohan D, Pittman CU, Steele PH. Pyrolysis of wood/biomass for bio-oil: a critical review. Energy Fuels 2006;20:848–89. https://doi.org/10.1021/ef0502397.

[36] Rioche C, Kulkarni S, Meunier FC, Breen JP, Burch R. Steam reforming of model compounds and fast pyrolysis bio-oil on supported noble metal catalysts. Appl Catal B Environ 2005;61:130–9. https://doi.org/10.1016/j.apcatb.2005.04.015.

[37] Fu M, Qi W, Xu Q, Zhang S, Yan Y. Hydrogen production from bio-oil model compounds dry (CO2) reforming over Ni/Al2O3catalyst. Int J Hydrogen Energy 2016;41:1494–501. https://doi.org/10.1016/j.ijhydene.2015.11.104.

[38] Ledesma EB, Campos C, Cranmer DJ, Foytik BL, Ton MN, Dixon EA, et al. Vapor-phase cracking of eugenol: Distribution of tar products as functions of temperature and residence time. Energy Fuels 2013;27:868–78. https://doi.org/10.1021/ef3018332.

[39] Manyà JJ, Azuara M, Manso JA. Biochar production through slow pyrolysis of different biomass materials: Seeking the best operating conditions. Biomass Bioenergy 2018;117:115–23. https://doi.org/10.1016/j.biombioe.2018.07.019.

[40] Robau-Sánchez A, Aguilar-Elguézabal A, Aguilar-Pliego J. Chemical activation of Quercus agrifolia char using KOH: Evidence of cyanide presence. Microporous

Mesoporous Mater 2005;85:331–339. https://doi.org/10.1016/j.micromeso.2005.07.003.

[41] Walton KS, Snurr RQ. Applicability of the BET method for determining surface areas of microporous metal-organic frameworks. J Am Chem Soc 2007;129:8552–6. https://doi.org/10.1021/ja071174k.

[42] Kim KC, Yoon TU, Bae YS. Applicability of using CO2 adsorption isotherms to determine BET surface areas of microporous materials. Microporous Mesoporous Mat 2016;224:294–301. https://doi.org/10.1016/j.micromeso.2016.01.003.

[43] Fang Q, Chen B, Lin Y, Guan Y. Aromatic and hydrophobic surfaces of wood-derived biochar enhance perchlorate adsorption via hydrogen bonding to oxygen-containing organic groups. Environ Sci Technol 2013;48:279–88. https://doi.org/10.1021/es403711y.

[44] Plaza MG, Pevida C, Arias B, Fermoso J, Casal MD, Martín CF, et al. Development of low-cost biomass-based adsorbents for postcombustion CO2 capture. Fuel 2009;88:2442–7. https://doi.org/10.1016/j.fuel.2009.02.025.

[45] Jung SH, Kim JS. Production of biochars by intermediate pyrolysis and activated carbons from oak by three activation methods using CO2. J Anal Appl Pyrolysis 2014;107:116–22. https://doi.org/10.1016/j.jaap.2014.02.011.

[46] Remiro A, Valle B, Aguayo AT, Bilbao J, Gayubo AG. Operating conditions for attenuating Ni/La2O3- αAl2O3 catalyst deactivation in the steam reforming of bio-oil aqueous fraction. Fuel Process Technol 2013;115:222–32. https://doi.org/10.1016/j.fuproc.2013.06.003.

[47] Arregi A, Lopez G, Amutio M, Artetxe M, Barbarias I, Bilbao J, et al. Role of operating conditions in the catalyst deactivation in the in-line steam reforming of volatiles from biomass fast pyrolysis. Fuel 2018;216:233–44. https://doi.org/10.1016/j.fuel.2017.12.002.

[48] Sueyasu T, Oike T, Mori A, Kudo S, Norinaga K, Hayashi JI. Simultaneous steam reforming of tar and steam gasification of char from the pyrolysis of potassium-loaded woody biomass. Energy Fuels 2012;26:199–208. https://doi.org/10.1021/ef201166a.

[49] Feng D, Zhao Y, Zhang Y, Sun S, Meng S, Guo Y, et al. Effects of K and Ca on reforming of model tar compounds with pyrolysis biochars under H2O or CO2. Chem Eng J 2016;306:422–32. https://doi.org/10.1016/j.cej.2016.07.065.

[50] Xu M, Sheng C. Influences of the Heat-Treatment Temperature and Inorganic Matter on Combustion Characteristics of Cornstalk Biochars. Energy Fuels 2012;26:209–18. https://doi.org/10.1021/ef2011657.

[51] Hosokai S, Kumabe K, Ohshita M, Norinaga K, Li CZ, Hayashi J ichiro. Mechanism of decomposition of aromatics over charcoal and necessary condition for maintaining its activity. Fuel 2008;87:2914–22. https://doi.org/10.1016/j.fuel.2008.04.019.

[52] Hu M, Laghari M, Cui B, Xiao B, Zhang B, Guo D. Catalytic cracking of biomass tar over char supported nickel catalyst. Energy 2018;145:228–37. https://doi.org/10.1016/j.energy.2017.12.096.

[53] Cao Y, Gao Z, Jin J, Zhou H, Cohron M, Zhao H, et al. Synthesis gas production with an adjustable H2/CO ratio through the coal gasification process: Effects of coal ranks and methane addition. Energy Fuels 2008;22:1720–30.

https://doi.org/10.1021/ef7005707.

[54] Yuan H, Wu S, Yin X, Huang Y, Guo D, Wu C. Adjustment of biomass product gas to raise H2/CO ratio and remove tar over sodium titanate catalysts. Renew Energy 2018;115:288–98. https://doi.org/10.1016/j.renene.2017.08.025.

Table 1

Summary of the nomenclature used in the present study for wheat straw-derived carbon materials.

Material	*Further treatment*
RW	Raw pyrolysis biochar
BC	Raw biochar devolatilized up to 800 °C under N_2
CAC	Chemically activated biochar through impregnation of a K_2CO_3 aqueous solution (2 M) and subsequent heating up to 700 °C under N_2
PAC15	Physically activated with CO_2 at 800 °C up to a degree of burn-off of 15%
PAC30	Physically activated with CO_2 at 800 °C up to a degree of burn-off of 30%
PAC40	Physically activated with CO_2 at 800 °C up to a degree of burn-off of 40%

Table 2

Summary of the operating conditions used for the conducted experiments.

	Cracking	*Steam Reforming*	*Steam and dry reforming*	
Liquid fed	Model mixture	Model mixture + H_2O	Model mixture + H_2O	Pyrolysis oil (aqueous fraction)
Gas fed	N_2	N_2	Mixture of N_2 and CO_2 (p_{CO2} of 10, 20 and 30 kPa)	Mixture of N_2 and CO_2 (p_{CO2} of 20 kPa)
Catalyst	All	PAC40	PAC40	PAC40
Temperature (°C)	700	600, 650, 700, 750	750	750
GHSV (h^{-1})	19500	12000, 14500, 19500, 35000	14500	14500

Table 3

Specific surface areas and pore volumes of the carbon materials involved in the present study.

Material	*Apparent specific surface area (m^2 g^{-1})*		*Specific pore volume (cm^3 g^{-1})*			
	S_{BET}[a]	S_{BET}[b]	V_t	V_{mic}	V_{mes}	V_{ultra}
BC	1.68	72.4	ND	ND	ND	0.023
CAC	89.0	291	0.045	0.031	0.009	0.119
PAC15	455	351	0.196	0.145	0.010	0.141
PAC30	637	414	0.283	0.234	0.018	0.140
PAC40	815	440	0.366	0.306	0.024	0.151

[a] Determined from N_2 adsorption data a –196 °C.

[b] Determined from CO_2 adsorption data a 0 °C.

Table 4

Main reactions occurring during the upgrading of pyrolysis vapors.

No.	*Reaction*	ΔH^0 *(kJ mol^{-1})*
1	$C_nH_mO_k \rightarrow C_xH_yO_z$ + *gases* (H_2, H_2O, CO_2, CO, CH_4, C_2H_x, C_3H_y,...) + *coke*	> 0
2	$C_nH_mO_k + (2n-k)\,H_2O \rightleftarrows nCO_2 + \left(2n + \frac{m}{2} - k\right)H_2$	173.6[c]
3	$C_nH_mO_k + (n-k)\,H_2O \rightleftarrows nCO + \left(n + \frac{m}{2} - k\right)H_2$	255.9[c]
4	$CO + H_2O \rightleftarrows CO_2 + H_2$	–41.2
5	$C_nH_mO_k + (n-k)\,CO_2 \rightleftarrows (2n-k)\,CO + \left(\frac{m}{2}\right)H_2$	297.0[c]
6	$C + H_2O \rightleftarrows CO + H_2$	131.3
7	$C + CO_2 \rightleftarrows 2CO$	172.5
8	$CO + 3H_2 \rightleftarrows CH_4 + H_2O$	–205.8
9	$CO_2 + 4H_2 \rightleftarrows CH_4 + H_2O$	77.2
10	$C + 2H_2 \rightleftarrows CH_4$	–74.5

[c] Referred to ethanol (C_2H_6O).

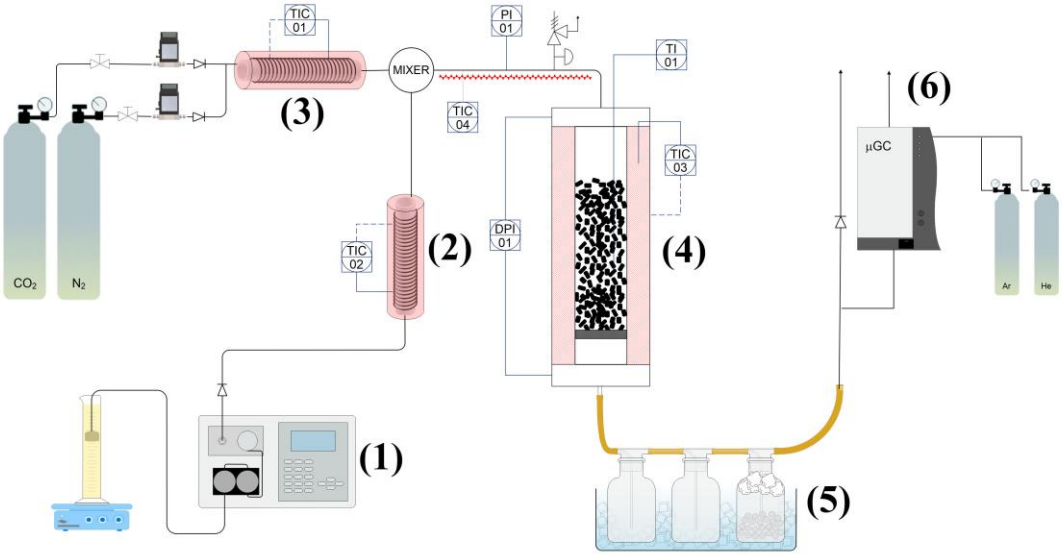

Fig. 1. Scheme of the experimental device used for cracking and reforming experiments: HPLC pump (1); evaporator (2); gas pre-heater (3); fixed-bed reactor and furnace (4); condensation train (5); and µ-GC analyzer (6).

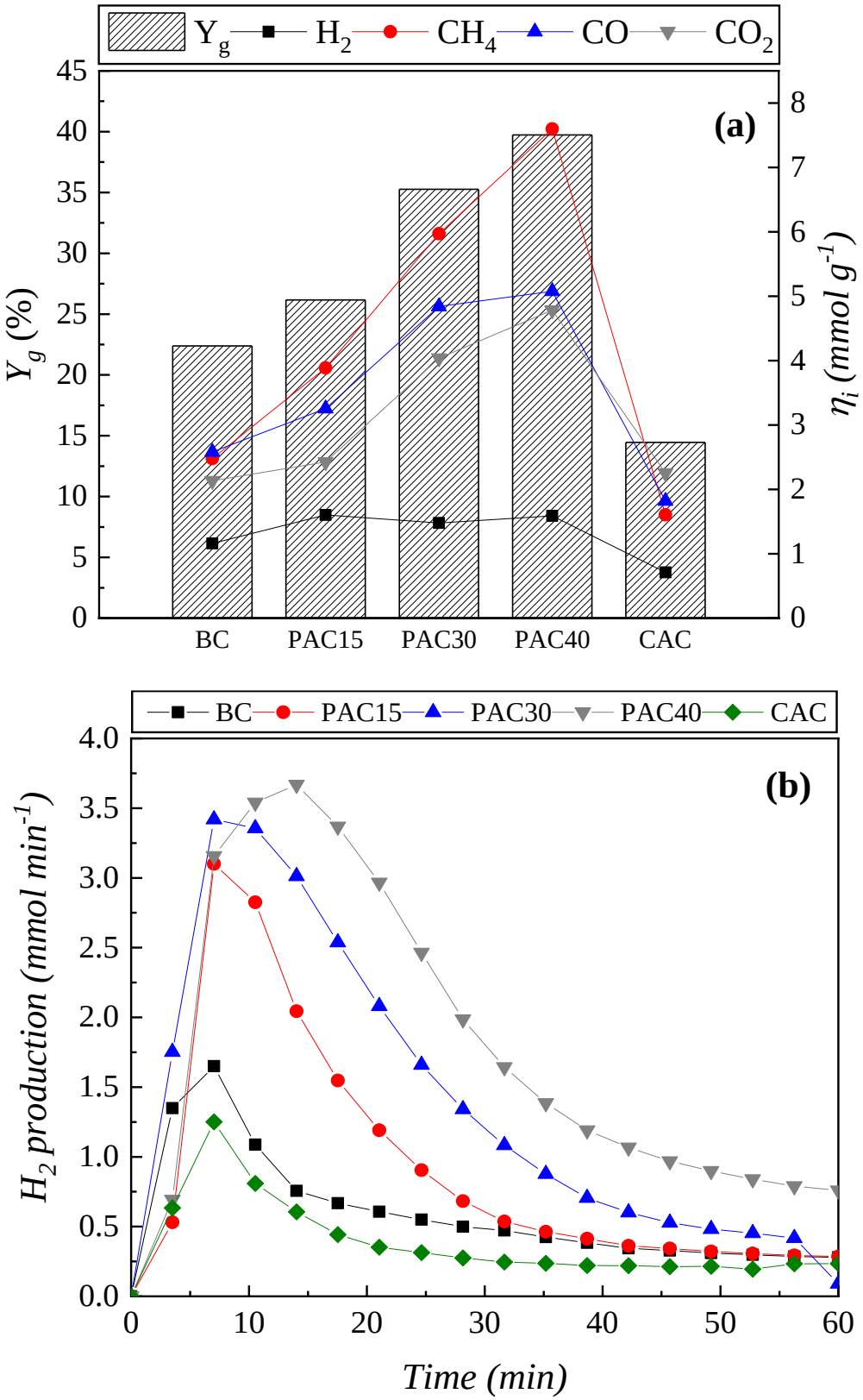

Fig. 2. Results obtained from the catalytic cracking experiments (700 °C and GHSV of 19500 h^{-1}): total gas production (Y_g) and yields of gaseous species (a), and time evolution of the H_2 production rate (b).

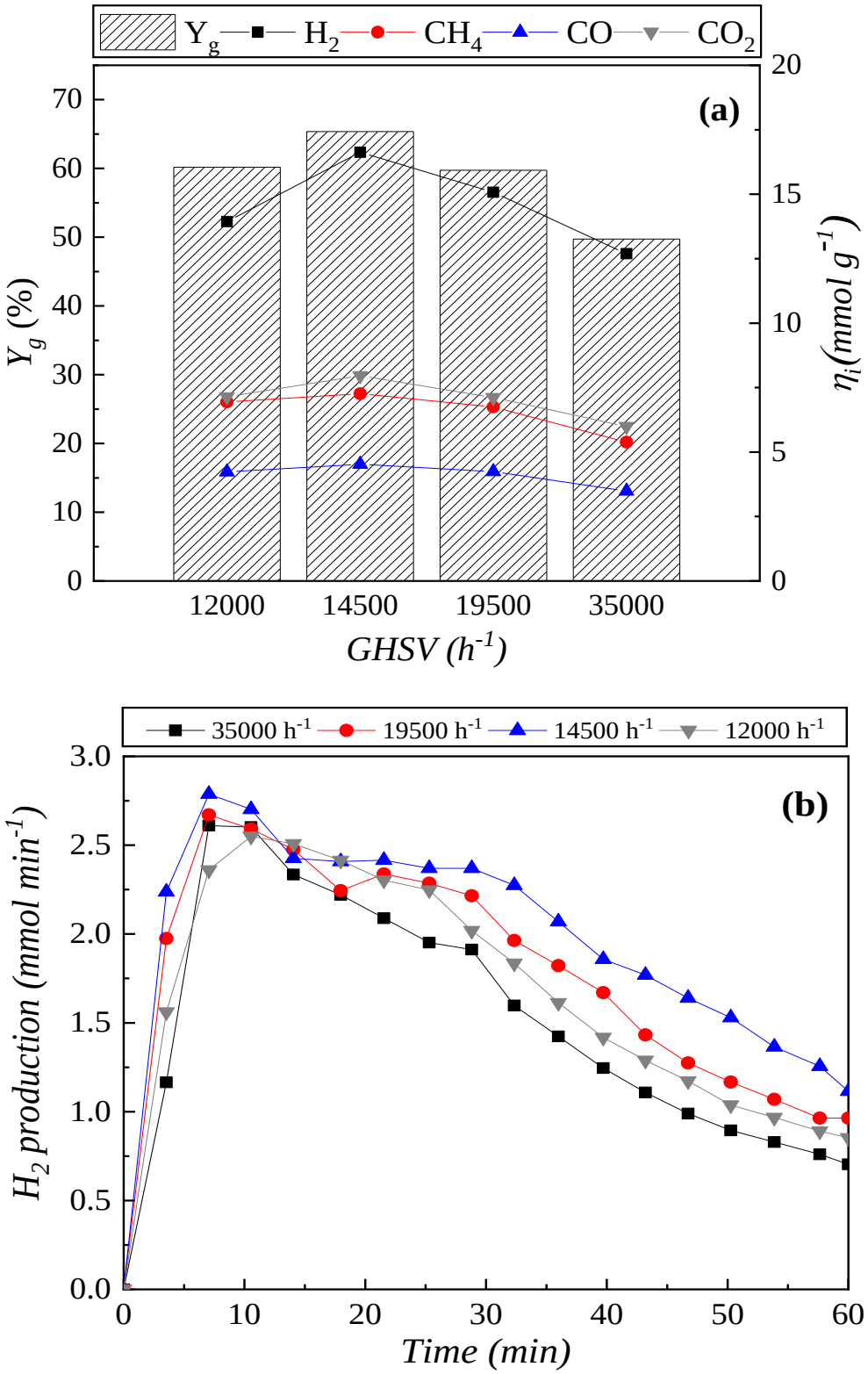

Fig. 3. Results obtained from the catalytic steam reforming experiments conducted at 700 °C, using the PAC40 material, and at different GHSV values: total gas production (Y_g) and yields of gaseous species (a), and time evolution of the H_2 production rate (b).

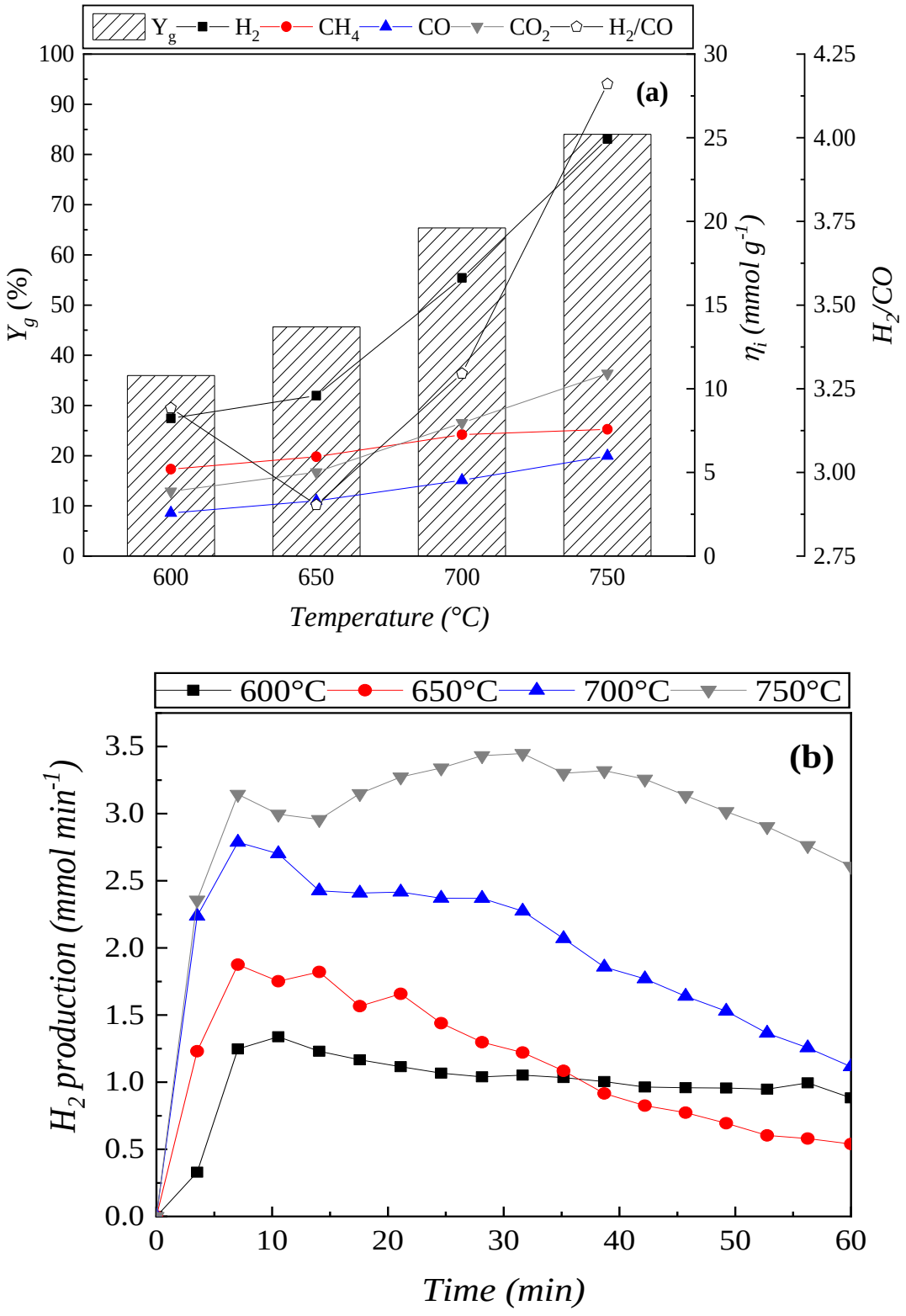

Fig. 4. Results obtained from the catalytic steam reforming experiments conducted at a GHSV of 14500 h^{-1}, using the PAC40 material, and at different bed temperatures: total gas production (Y_g) and yields of gaseous species (a), and time evolution of the H_2 production rate (b).

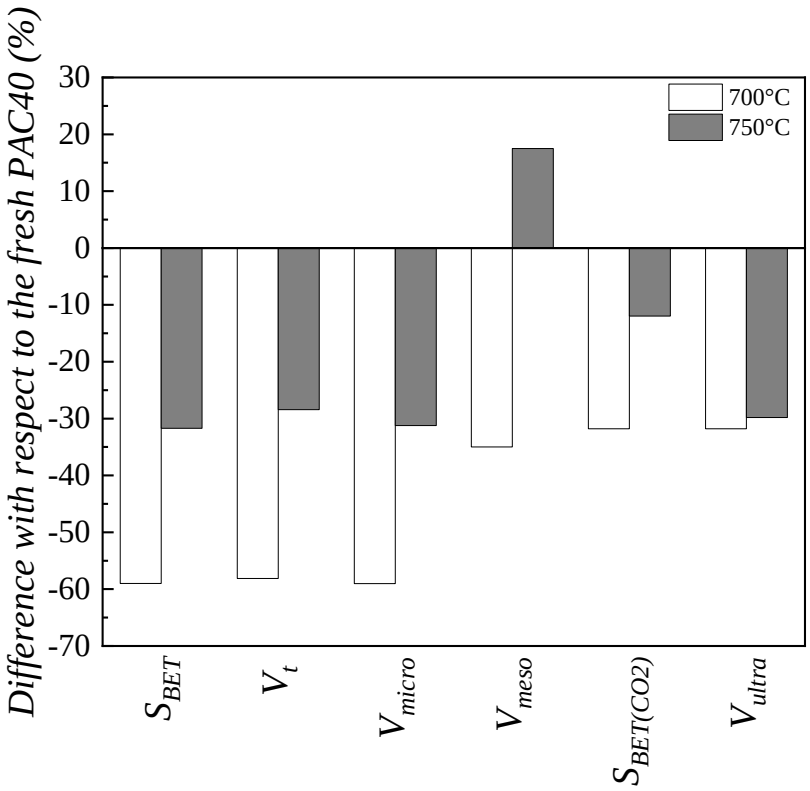

Fig. 5. Differences in textural properties between the fresh and spent PAC40 materials from the SR tests at 700 and 750 °C.

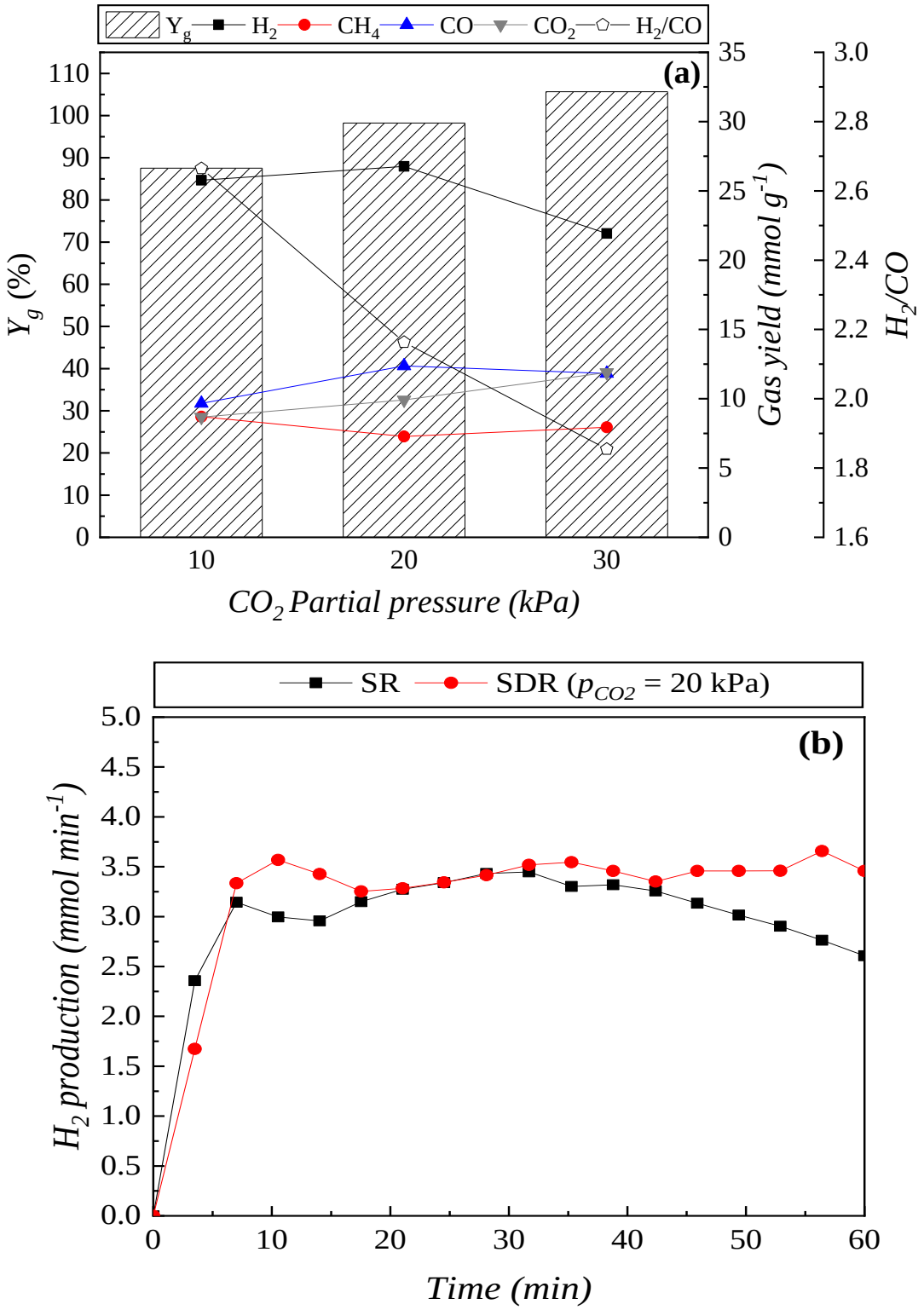

Fig. 6. Results obtained from the catalytic steam and dry reforming experiments conducted using the PAC40 material at 750 °C, a GHSV of 14500 h^{-1}, and at different partial pressures of CO_2 in the feed gas stream: total gas production (Y_g) and yields of gaseous species (a), and time evolution of the H_2 production rate for the best SR and SDR conditions (b).

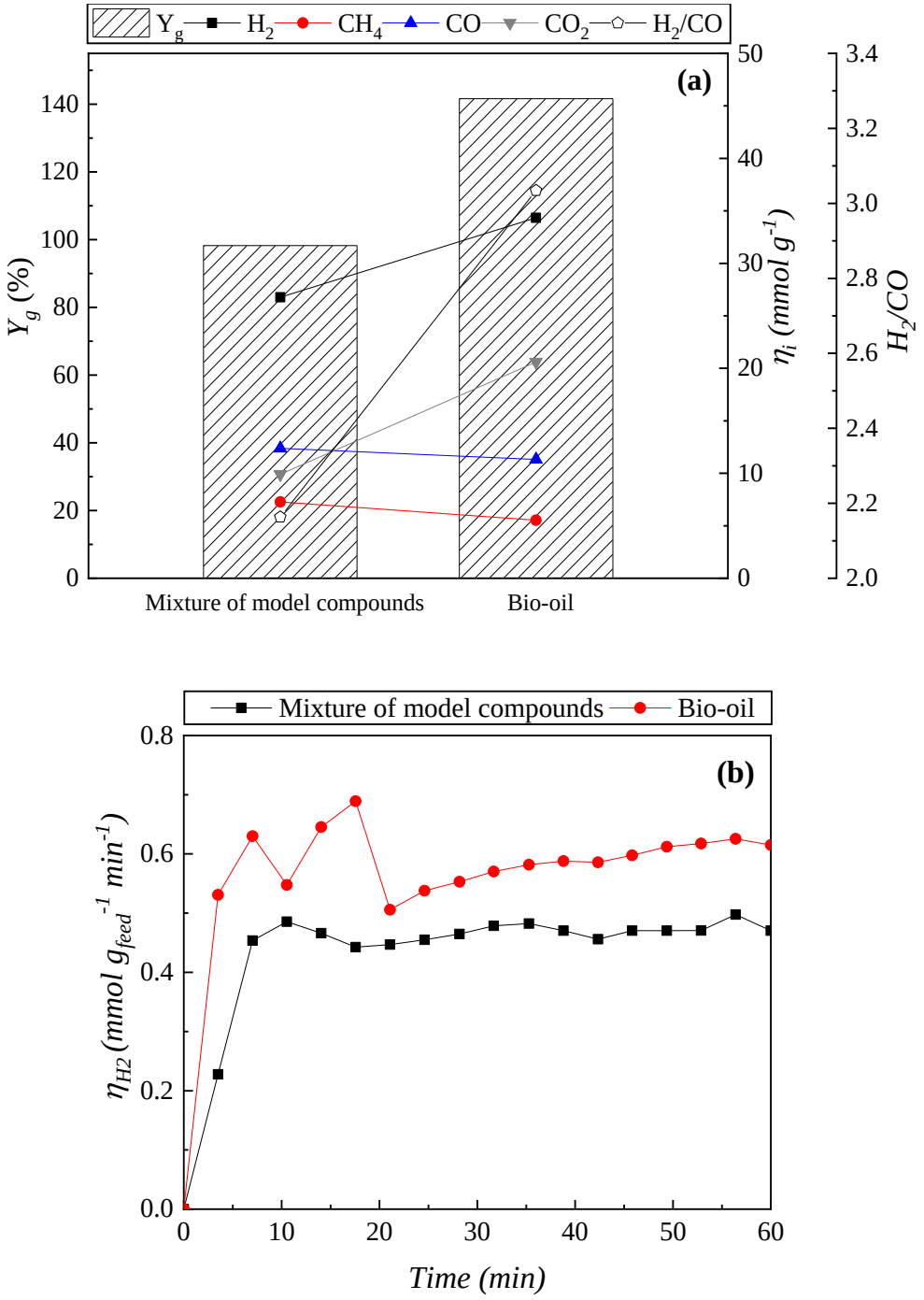

Fig. 7. Comparison of the results obtained from SDR tests of the mixture of model compounds and the real bio-oil sample: total gas production (Y_g) and yields of gaseous species (a), and time evolution of the instantaneous yield of H_2 (b). Both tests were conducted using the PAC40 material at 750 °C, a GHSV of 14500 h^{-1}, and a CO_2 partial pressure of 20 kPa.

Appendix A. Supplementary Data

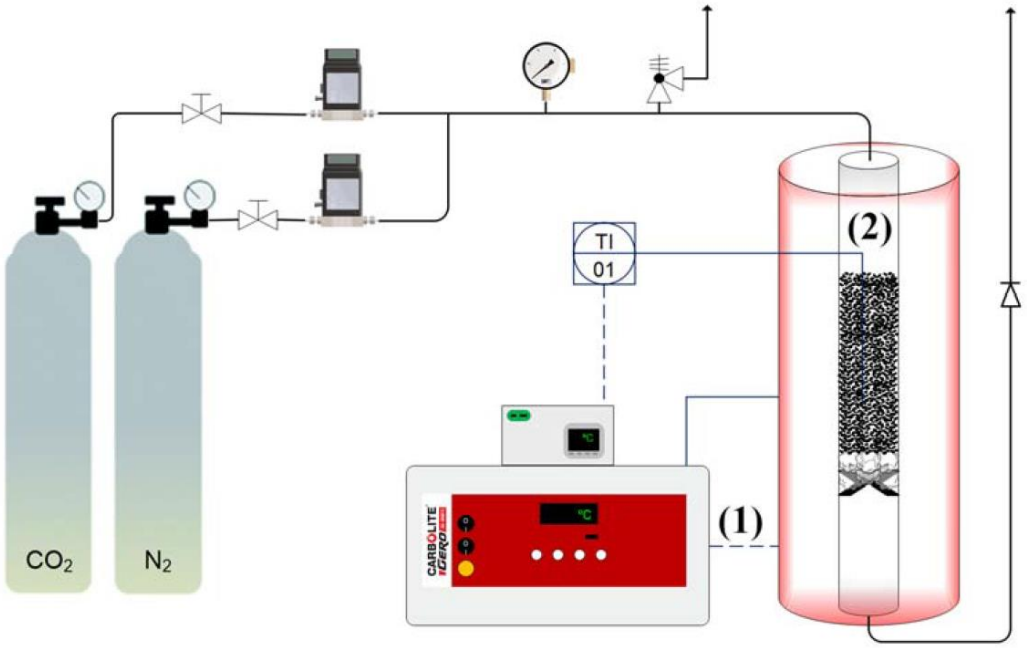

Fig. A.1. Schematic representation of the activation set-up used for the production of physically and chemically activated biochars: furnace (1) and quartz reactor (2).

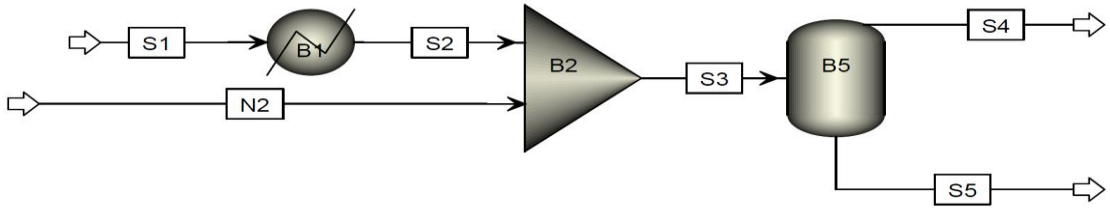

Fig A.2. Flowsheet of the simulation case conducted using Aspen Plus.

The simulation was carried out using the "NRTL" fluid package. The blocks B1, B2 and B3 in Fig. A.2 correspond to a heater, a mixer, and a flash separator; respectively. The results showed that non-negligible mass flow rates of acetic acid, ethanol and acetone are lost in the stream S4 (see Table A.1).

Table A.1

Summary of the simulation results.

	Stream					
	N2	*S1*	*S2*	*S3*	*S4*	*S5*
Phase	Vapor	Liquid	Vapor	Vapor	Vapor	Liquid
Temperature (°C)	300	20	183	255	25	25
Pressure (kPa)	101.3	101.3	101.3	101.3	101.3	101.3
Mass flow rate (g h^{-1})	37.52	13.58	13.58	51.10	42.82	8.276
Acetic acid (g h^{-1})	0.000	3.395	3.395	3.395	0.710	2.685
Ethanol (g h^{-1})	0.000	3.395	3.395	3.395	1.764	1.631
Acetone (g h^{-1})	0.000	3.395	3.395	3.395	2.832	0.563
Eugenol (g h^{-1})	0.000	3.395	3.395	3.395	0.001	3.394
N_2 (g h^{-1})	37.52	0.000	0.000	37.52	37.51	0.003

	Distribution of model compounds in streams S4 and S5	
	S4 (Vapors) wt. %	*S5 (Liquids) wt. %*
Acetic acid	20.90	79.10
Ethanol	51.95	48.05
Acetone	83.43	16.57
Eugenol	0.030	99.97

Table A.2

Results from the repeatability tests for the used experimental set-up. The repeated experiment (steam and dry reforming of the mixture of model compounds) was conducted using the PAC40 catalyst, at 700 °C, at a GHSV of 14500 h^{-1}, and a N_2/CO_2 feed gas ratio of 1:1 (v/v).

	Y_g	η_{H2}	η_{CH4}	η_{CO}
Replicate 1	38.0	12.4	6.55	8.19
Replicate 2	35.0	11.7	5.88	7.52
Replicate 3	37.8	11.8	6.47	8.26
Mean	36.9	12.0	6.30	7.99
Standard deviation	1.68	0.38	0.36	0.41
Coefficient of variation (%)	4.54	3.16	5.81	5.11

Table A.3

Proximate and elemental analyses of wheat straw pellets and non-activated biochar.

	Wheat straw	*RW*
Proximate analysis (wt. %)		
Moisture	7.60 ± 0.11	1.47 ± 0.06
Volatiles	74.8 ± 0.87	16.2 ± 0.71
Ashes	4.23 ± 0.28	13.5 ± 0.11
Fixed carbon	13.3 ± 1.17	68.8 ± 0.54
Elemental Analysis (wt. % in dry-ash-free basis)		
C	44.1 ± 0.10	93.2 ± 0.03
H	6.30 ± 0.02	4.13 ± 0.05
N	0.62 ± 0.02	1.98 ± 0.02
O[a]	48.97	0.71
Atomic H:C ratio	1.71	0.53
Atomic O:C ratio	0.83	0.0057
Inorganic matter (wt. % of ash)[b]		
K	*4.22*	*12.3*
Ca	*2.38*	*6.78*
Si	*1.51*	*4.53*
Cl	*0.292*	*0.658*
Mg	*0.167*	*0.482*
Fe	*0.0760*	*0.275*
Al	*0.0481*	*0.0817*
Pb	*0.0400*	*0.0321*

[a] Calculated by difference.
[b] Results of the XRF analysis

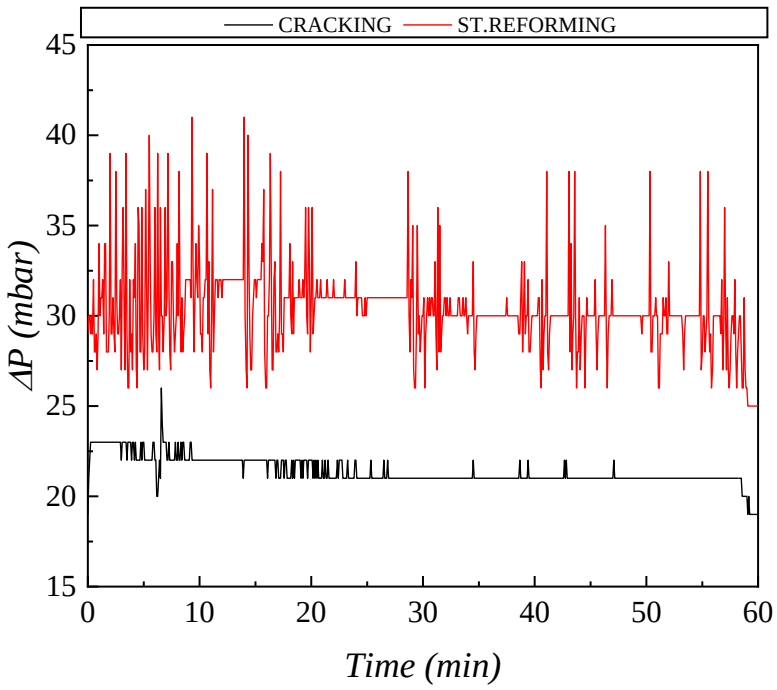

Fig. A.3. Comparison of the pressure drop (*ΔP*) evolution during the catalytic cracking and steam reforming tests for the PAC40 catalysts at 700 °C and at a GHSV of 19500 h^{-1}.